

## RESEARCH ARTICLE SUMMARY

## HUMAN FERTILITY

# The mechanism of acentrosomal spindle assembly in human oocytes

Tianyu Wu<sup>†</sup>, Jie Dong<sup>†</sup>, Jing Fu<sup>†</sup>, Yanping Kuang<sup>†</sup>, Biaobang Chen, Hao Gu, Yuxi Luo, Ruihuan Gu, Meiling Zhang, Wen Li, Xi Dong, Xiaoxi Sun\*, Qing Sang\*, Lei Wang\*

**INTRODUCTION:** Spindle assembly is essential for ensuring accurate chromosome transmission in both meiosis and mitosis. In somatic cells, mitotic spindle assembly is mediated by duplicated centrosomes, but canonical centrosomes are absent in the oocytes of many species. In rodents, acentriolar microtubule organizing centers (aMTOCs) are responsible for meiotic spindle assembly, but it has long been supposed that human oocytes lack prominent aMTOCs on the meiotic spindle, and the exact mechanism of acentrosomal spindle assembly in human oocytes has remained unclear.

**RATIONALE:** Microtubule nucleation and ensuring spindle assembly are core events regulating oocyte nuclear maturation. To identify the potential proteins driving spindle microtubule nucleation in human oocytes, we systematically localized 86 human centrosome and microtubule-related proteins by immunofluorescence or three-dimensional high-resolution live cell imaging in more than 2000 human oocytes. We then tracked the dynamic migration of identified microtubule nucleators at different time points before and after nuclear envelope breakdown (NEBD). We further down-regulated corresponding proteins to confirm their role in microtubule nucleation and spindle assembly. Given that spindle microtubule nucleation defects result in impaired spindle assembly and abnormal oocyte maturation, we screened for mutations in genes encoding com-

ponents of microtubule nucleators in a cohort of 1394 infertile female patients characterized by oocyte maturation arrest.

**RESULTS:** First, we found that in human oocytes the nucleation of spindle microtubules is initiated from kinetochores from 2 to 4 hours after NEBD. We showed the process of spindle microtubules nucleating from kinetochores in human oocytes. We then found that there are 43 proteins localized in the meiotic spindle, among which four proteins—centriolar coiled-coil protein 110 (CCP110), cytoskeleton-associated protein 5 (CKAP5), disrupted in schizophrenia 1 (DISC1), and transforming acidic coiled-coil-containing protein 3 (TACC3)—exhibited both kinetochore and spindle microtubule localization. The localization of the four proteins was notably different from their localization in human mitotic cells and in mouse oocytes. Together, the four proteins formed an unusual structure that was surrounded by microtubules in human germinal vesicle (GV) oocytes just before NEBD. We refer to this potential nucleating structure as the human oocyte microtubule organizing center (huoMTOC). We found that a single huoMTOC is formed at the cortex of human GV oocytes and migrates to the nuclear envelope before NEBD. After NEBD, the huoMTOC becomes fragmented and is recruited to kinetochores to initiate spindle microtubule nucleation. Down-regulation of huoMTOC components caused considera-

bly impaired spindle microtubule nucleation and spindle assembly in human oocytes. This structure was not detected in the oocytes of other mammalian species such as mice and pigs. We finally identified two oocyte maturation arrest patients with compound heterozygous mutations in the key huoMTOC component TACC3. All mutations disrupted the normal function of TACC3, resulting in the absence of the huoMTOC structure and completely impaired spindle assembly in the patients' oocytes.

**CONCLUSION:** Our study shows that human oocytes possess an aMTOC-like structure, the huoMTOC, that serves as a major site of microtubule nucleation and is required for spindle assembly. The huoMTOC shows drastically different characteristics in terms of number, localization, and composition compared with aMTOCs in mouse oocytes. These findings suggest that a distinct mechanism for the initiation of microtubule nucleation and spindle assembly has evolved in human oocytes. We found that mutations in TACC3 cause defects in spindle assembly by disrupting the structure of the huoMTOC, which leads to clinical oocyte maturation arrest. This suggests that the huoMTOC might be an important biomarker for evaluating the quality of human oocytes.

Our discovery of huoMTOC provides insights into the physiological mechanism of microtubule nucleation and spindle assembly in human oocytes. These findings also improve our understanding of the pathological mechanisms of oocyte maturation arrest. ■

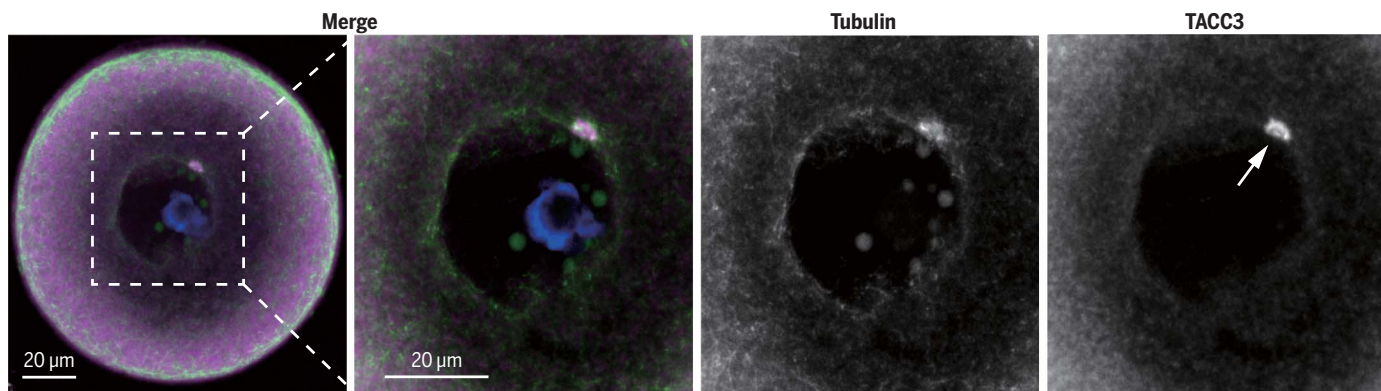
The list of author affiliations is available in the full article online.

\*Corresponding author. Email: wangleiwanglei@fudan.edu.cn (L.W.); sangqing@fudan.edu.cn (Q.S.); xiaoxi\_sun@aliyun.com (X.S.)

†These authors contributed equally to this work.

Cite this article as T. Wu et al., *Science* **378**, eabq7361 (2022). DOI: 10.1126/science.abq7361

**S** READ THE FULL ARTICLE AT  
<https://doi.org/10.1126/science.abq7361>



**The huoMTOC structure in a human oocyte.** The human GV oocyte shown here was matured for ~5 hours and fixed for immunofluorescence before NEBD. The huoMTOC (TACC3, magenta) was surrounded by numerous microtubules (green) on the nuclear envelope. The dashed square shows the magnification region. The arrow highlights the huoMTOC.

## RESEARCH ARTICLE

## HUMAN FERTILITY

# The mechanism of acentrosomal spindle assembly in human oocytes

Tianyu Wu<sup>1†</sup>, Jie Dong<sup>1†</sup>, Jing Fu<sup>2†</sup>, Yanping Kuang<sup>3†</sup>, Biaobang Chen<sup>4</sup>, Hao Gu<sup>1</sup>, Yuxi Luo<sup>1</sup>, Ruihuan Gu<sup>2</sup>, Meiling Zhang<sup>5</sup>, Wen Li<sup>5</sup>, Xi Dong<sup>6</sup>, Xiaoxi Sun<sup>2\*</sup>, Qing Sang<sup>1\*</sup>, Lei Wang<sup>1\*</sup>

Meiotic spindle assembly ensures proper chromosome segregation in oocytes. However, the mechanisms behind spindle assembly in human oocytes remain largely unknown. We used three-dimensional high-resolution imaging of more than 2000 human oocytes to identify a structure that we named the human oocyte microtubule organizing center (huoMTOC). The proteins TACC3, CCP110, CKAP5, and DISC1 were found to be essential components of the huoMTOC. The huoMTOC arises beneath the oocyte cortex and migrates adjacent to the nuclear envelope before nuclear envelope breakdown (NEBD). After NEBD, the huoMTOC fragments and relocates on the kinetochores to initiate microtubule nucleation and spindle assembly. Disrupting the huoMTOC led to spindle assembly defects and oocyte maturation arrest. These results reveal a physiological mechanism of huoMTOC-regulated spindle assembly in human oocytes.

**S**pindle assembly is essential for ensuring accurate chromosome transmission in both mitosis and meiosis (1, 2). In somatic cells, mitotic spindle assembly is mediated via duplicated centrosomes, which consist of two centrioles surrounded by the pericentriolar material (PCM) (3, 4). Centrosomes are the major microtubule organizing centers (MTOCs) in mitotic cells, and they are responsible for microtubule nucleation and spindle pole organization of the centrosomal spindle (5, 6).

Unlike somatic cells, canonical centrosomes are absent in the oocytes of many species (7–11). Instead, acentriolar MTOCs (aMTOCs) are observed in frog (12) and mouse (13–15) oocytes, whereas no MTOC structures are found in the *Drosophila* (16) or *Caenorhabditis elegans* (17) oocytes. The difference suggests that the mechanisms of female meiotic spindle assembly are not conserved between species. The aMTOC-directed meiotic spindle assembly was only elucidated in mouse oocytes (15, 18, 19).

Mouse aMTOCs lack centrioles but contain partial centrosomal proteins such as pericentrin (14),  $\gamma$ -tubulin (20), CEP192 (18), and NEDD1 (21). Upon meiotic resumption after prophase I arrest, multiple aMTOCs initiate microtubule nucleation around the nuclear envelope in mouse germinal vesicle (GV) oocytes. After nuclear envelope breakdown (NEBD), aMTOCs are clustered and then concentrated at the spindle poles for bipolar spindle organization (15, 18, 19).

A mechanistic understanding of meiotic spindle assembly in human oocytes, on the other hand, remains elusive (2). It is only known that the spindle microtubule nucleation in human oocytes is mediated by chromosomes and promoted by guanosine triphosphate (GTP)-bound Ran (RanGTP) (22). Subsequently, a multipolar spindle is assembled as an intermediate, and then the spindle poles are merged to form a bipolar spindle (22). However, human oocytes lack detectable aMTOCs at the meiotic spindle poles (22, 23), and thus the exact mechanism of acentrosomal spindle assembly in human oocytes remains unclear.

## Results

### Spindle microtubules are nucleated from kinetochores in human oocytes

A previous study implied that spindle microtubules emanate from the kinetochores in human oocytes (22), and this phenomenon was also observed in our immunofluorescent results in early prometaphase oocytes (fig. S1). This suggests that kinetochores may serve as the microtubule nucleation sites in human oocytes. However, the dynamic process of how spindle microtubules were originally nucleated from kinetochores was not delineated. Thus, we first observed the process of microtubule

nucleation in live human oocytes by using three-dimensional (3D) high-resolution time-lapse imaging (Fig. 1A). Human GV oocytes were co-injected with mRNA encoding fluorescently fused histone H2B (mCherry) and centromere protein B (CENPB) (mClover3) to visualize chromosomes and kinetochores, respectively. Combined with fluorescent proteins, SiR-tubulin (a dye with far-red fluorescence) was used to label microtubules before oocyte maturation (24). According to our three-channel time-lapse images, a microtubule cluster (dashed square) derived from a GV oocyte was observed proximal to chromosomes upon NEBD and disassembled in the first few hours of meiosis I (Fig. 1A). Apart from the microtubules (light-gray curve, bottom panel) derived from the GV oocyte, a few nascent microtubules (dark-gray curve, bottom panel) were detected by microscopy after NEBD (Fig. 1A).

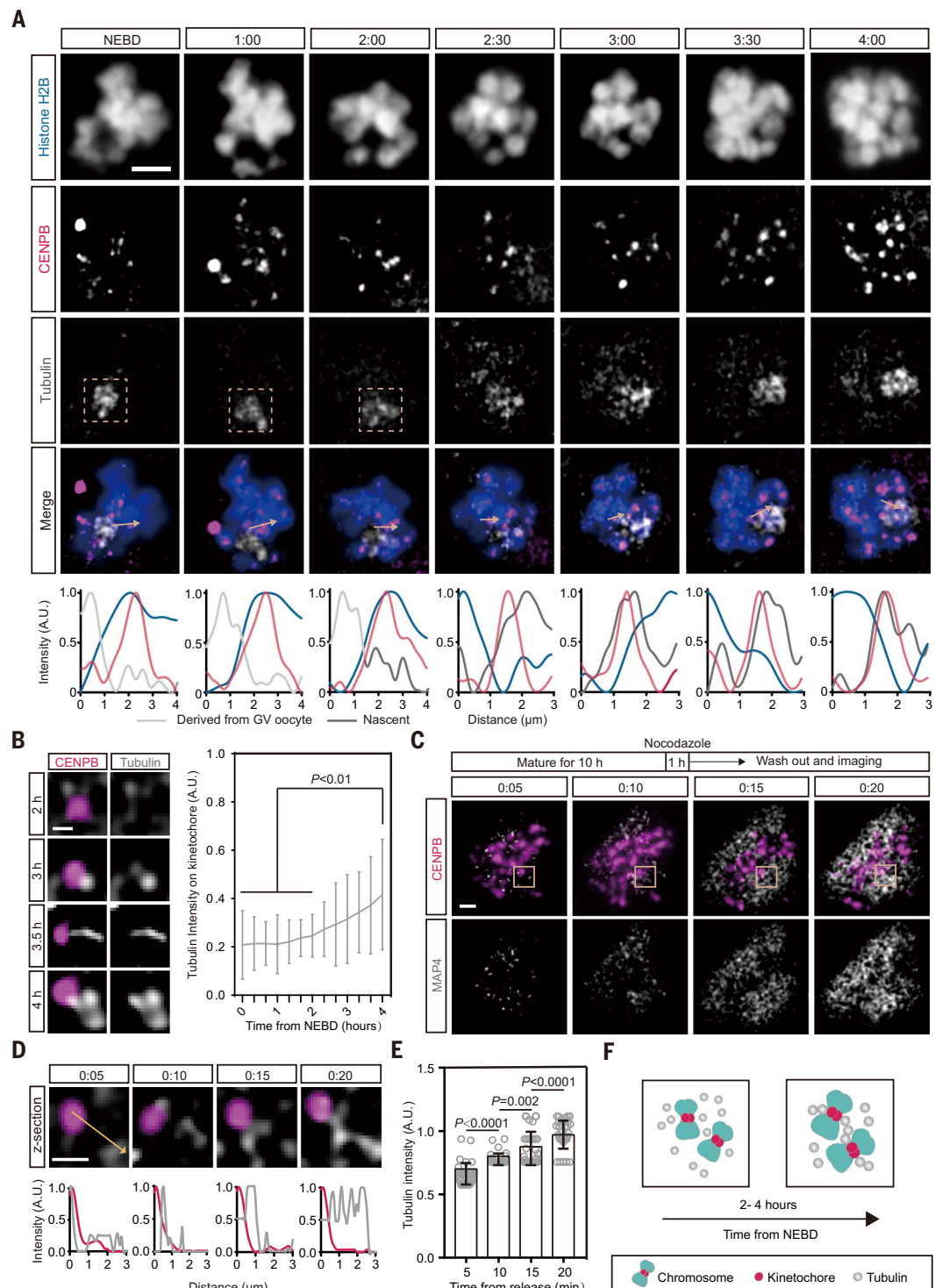
To confirm that the nascent microtubules were polymerized from kinetochores, we evaluated the tubulin intensity around kinetochores over time after NEBD. The intensity of microtubules (tubulin) and chromosomes (H2B) was measured around the representative kinetochores (Fig. 1A, arrows). The nascent microtubules (dark-gray curve) were hardly observed at the beginning of meiosis in human oocytes (0 to 2 hours after NEBD). With the disassembly of the derived microtubule cluster (light-gray curve), the fluorescent tubulins began to concentrate at the kinetochores starting at ~2 hours after NEBD (Fig. 1, A and B). According to three-channel time-lapse imaging, the fluorescence of nascent microtubules (dark-gray curve) overlapped primarily with kinetochores (red curve) from 2 to 2.5 hours after NEBD and consistently throughout the beginning of meiosis I (2 to 4 hours after NEBD) (Fig. 1A). However, the fluorescence of nascent microtubules (dark-gray curve) did not consistently overlap with chromosomes (blue curve), suggesting that the nascent microtubules primarily polymerized from the kinetochores rather than other regions of the chromosomes (Fig. 1A). Along with meiotic maturation, microtubules were nucleated slowly but continuously (Fig. 1, A and B), and the stable microtubules with high tubulin intensity could be observed on kinetochores starting at 3 hours after NEBD (Fig. 1, A and B). These results suggest that in human oocytes, the nucleation of spindle microtubules is initiated from kinetochores starting at 2 to 4 hours after NEBD.

Next, to further confirm the nucleation of spindle microtubules on kinetochores, we treated live human metaphase I (MI) oocytes with a reversible microtubule inhibitor (nocodazole) and tracked the dynamic recovery of microtubule nucleation immediately after nocodazole was washed out (Fig. 1C). Microtubules and kinetochores were marked by

<sup>1</sup>Institute of Pediatrics, Children's Hospital of Fudan University, State Key Laboratory of Genetic Engineering, Institutes of Biomedical Sciences, Shanghai Key Laboratory of Medical Epigenetics, Fudan University, Shanghai 200032, China. <sup>2</sup>Shanghai Ji Ai Genetics and IVF Institute, Obstetrics and Gynecology Hospital, Fudan University, Shanghai 200011, China. <sup>3</sup>Department of Assisted Reproduction, Shanghai Ninth People's Hospital, Shanghai Jiao Tong University School of Medicine, Shanghai 200011, China. <sup>4</sup>NHC Key Lab of Reproduction Regulation, Shanghai Institute for Biomedical and Pharmaceutical Technologies, Fudan University, Shanghai 200032, China. <sup>5</sup>Center for Reproductive Medicine and Fertility Preservation Program, International Peace Maternity and Child Health Hospital, School of Medicine, Shanghai Jiao Tong University, Shanghai 200030, China. <sup>6</sup>Reproductive Medicine Center, Zhongshan Hospital, Fudan University, Shanghai 200032, China.

\*Corresponding author. Email: wangleiwanglei@fudan.edu.cn (L.W.); sangqing@fudan.edu.cn (Q.S.); xiaoxi\_sun@aliyun.com (X.S.)  
†These authors contributed equally to this work.

**Fig. 1. The dynamic process of spindle microtubules nucleating from kinetochores in human oocytes.** (A) Representative time-lapse images showing microtubule nucleation in human oocytes after NEBD. Blue, chromosomes (H2B-mCherry); gray, microtubules (SiR-tubulin); magenta, kinetochores (mClover-CENPB). The microtubule cluster was marked at 0 to 2 hours after NEBD (dashed squares). Representative kinetochores of each time point are shown in some z-sections. The intensity of chromosomes and microtubules was measured and plotted around representative kinetochores. The graphs in the bottom panel are the fluorescence profiles of H2B, tubulin, and CENPB across the representative kinetochores along the direction of the arrows in the merged images at each time point. The microtubules derived from GV oocytes (light-gray curves) and nascent microtubules (dark-gray curves) were distinguished at 2 hours after NEBD. The plotted intensity curves indicate the relative location of each fluorescent protein. Blue, chromosomes; gray, microtubules; magenta, kinetochores. A.U., arbitrary units. Scale bar, 5  $\mu$ m. (B) Representative images showing kinetochore nucleated microtubules at different time points. The intensity of the microtubules on kinetochores measured in (A) was compared between 2 and 4 hours after NEBD ( $n > 24$  kinetochores, significance of the differences in intensity was calculated by ANOVA and indicated on the graph). Scale bar, 2  $\mu$ m. (C) Representative time-lapse images (z-stack) showing microtubule nucleation after nocodazole washout in live human oocytes. Gray, microtubules (GFP-MAP4); magenta, kinetochores (mScarlet-CENPB). Flow diagram shows the sequence of experiments. Arrow indicates time-lapse imaging initiation. Time is given as hours:minutes after nocodazole washout. Scale bar, 5  $\mu$ m. (D) Single-slice images of boxed areas in (C). Time is given as hours:minutes after nocodazole washout. Scale bar, 2  $\mu$ m. Intensity of kinetochores and microtubules is indicated in the graphs. The bottom graphs are the fluorescence profiles of MAP4 (gray) and CENPB (magenta) proximal to the representative kinetochores along the direction of the yellow arrow. (E) The intensity of microtubules on kinetochores in (D) was measured and compared after nocodazole washout (significance was calculated by ANOVA). (F) Mechanistic model for microtubule nucleation in human oocytes. Time is after NEBD.



fluorescent microtubule-associated protein 4 (MAP4) and CENPB proteins, respectively. Initially, nocodazole completely disrupted the microtubules in human MI oocytes, and re-

polymerized microtubules were not detected on kinetochores until ~10 min after nocodazole was washed out. At that time, several nascent microtubules were observed near the kinetochores,

and some of them were emanating outward (Fig. 1C). The trajectory of microtubules was also shown in a single slice (Fig. 1D), and the representative kinetochore was nucleating

microtubules slowly and continuously, suggesting that nascent microtubules were nucleated from kinetochores (Fig. 1, D and E). Together, these results show the dynamic process of acentrosomal spindle microtubules nucleating from kinetochores in human oocytes (Fig. 1F).

#### Discovery of a specific microtubule nucleator in human oocytes

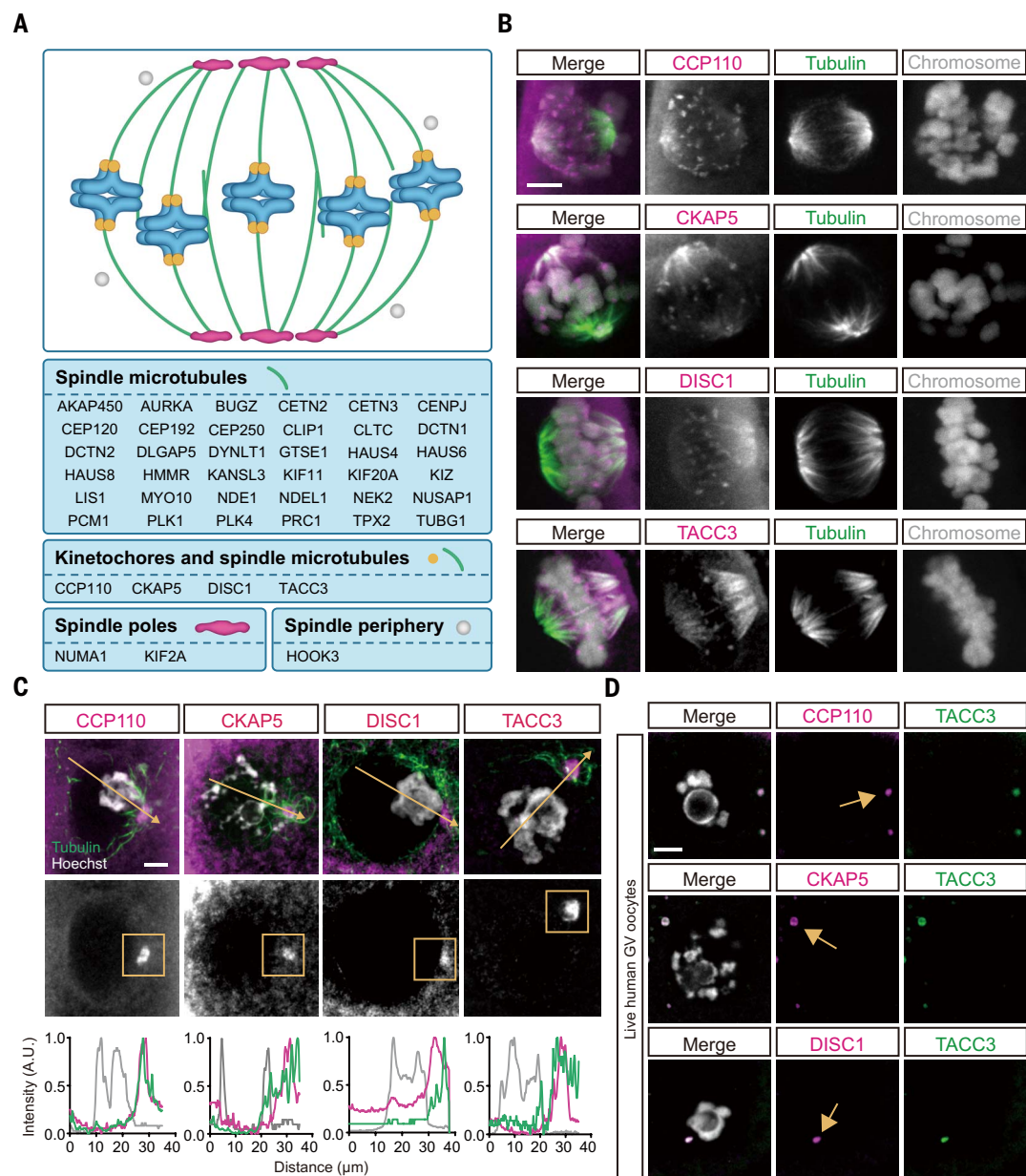
To identify the specific factors driving spindle microtubule nucleation from kinetochores in human oocytes, we localized 86 human centrosome and microtubule-related proteins by performing immunofluorescence in >1000 fixed human oocytes (Fig. 2A and figs. S2 and S3). These proteins were classified according to their function or localization in somatic

cells (21, 25, 26), but their localization in human oocytes was largely unknown. These proteins included 34 centrosomal proteins, 25 microtubule-associated proteins, 12 dynein-related proteins, five regulatory kinases or substrates, five spindle assembly factors, and five nuclear pore-related proteins (fig. S2). A total of 36 proteins were specifically localized on spindle microtubules, two proteins were concentrated on spindle poles, and one protein showed spindle periphery localization (Fig. 2A and fig. S3). Unexpectedly, four proteins—centriolar coiled-coil protein 110 (CCP110), cytoskeleton-associated protein 5 (CKAP5), disrupted in schizophrenia 1 (DISC1), and transforming acidic coiled-coil-containing protein 3 (TACC3)—exhibited both kineto-

chore and spindle microtubule localization (Fig. 2B), and such localization was consistent until the MII stage (fig. S4), which was notably different from their localization in human mitotic cells and in mouse oocytes (6, 21, 27–30).

CCP110 and DISC1 are centrosomal proteins that are involved in spindle assembly at the centrosomes of human mitotic cells and aMTOCs of mouse oocytes (6, 21, 27). CKAP5 and TACC3 are microtubule-associated proteins concentrated at centrosomes and microtubules in human mitotic cells during mitosis (28–30). Importantly, both CKAP5 and TACC3 have been reported to nucleate microtubules in vitro and in mitotic cells, respectively (31–34). These observations suggested that CCP110, CKAP5, DISC1, and TACC3 are potential

**Fig. 2. Identification of a microtubule nucleator in human oocytes.**



candidates for regulating microtubule nucleation and polymerization in human oocytes.

Subsequently, these proteins were monitored by immunofluorescence in human GV oocytes just before NEBD (fig. S5 and movie S1). Notably, each of the four proteins showed an unusual structure surrounded by microtubules. This structure was proximal to the nuclear envelope in human GV oocytes ~0 to 2 hours before NEBD (Fig. 2C), which was consistent with our observations of a microtubule cluster proximate to chromatin in human oocytes after NEBD (movie S2). To test whether these four proteins were colocalized, we overexpressed TACC3 (labeled with mScarlet) and the other three proteins (labeled with mClover3). As indicated in Fig. 2D, CCP110, CKAP5, and DISC1 were all colocalized with TACC3, implying that the four proteins belong to the same structure. To examine the interactions among these proteins, coimmunoprecipitation was performed in human embryonic kidney 293T (HEK293T) cells transfected with plasmids containing the corresponding genes. As a result, CCP110, CKAP5, and DISC1 all interacted directly with TACC3, whereas the negative control GDF9 had no interaction with TACC3 (fig. S6). This suggests that the four proteins are all components of the same structure. In addition, a dense microtubule cluster was observed around this structure in human GV oocytes, which caused asymmetrical microtubule distribution around the nuclear envelope prior to NEBD (Fig. 2C). Given these features, we refer to this potential nucleating structure as the human oocyte microtubule organizing center (huoMTOC). This structure was not detected in the oocytes of other mammalian species such as mice and pigs (fig. S7), suggesting the specificity of this structure in human oocytes.

#### **The huoMTOC is essential for microtubule nucleation**

According to the transcriptional landscape data of human oocytes in public databases (23), *TACC3* shows overwhelmingly higher expression (more than 29-fold) than *CCP110*, *CKAP5*, and *DISC1*, implying its potential key role in the huoMTOC. We therefore tried to disrupt the huoMTOC by knocking down *TACC3* by injecting the corresponding short-interfering RNAs (siRNAs) into human GV oocytes (fig. S8). The integrity of the huoMTOC was evaluated by immunofluorescence for CCP110, CKAP5, DISC1, and TACC3. As expected, no nucleating structures were detected, demonstrating the complete disruption of the huoMTOC upon TACC3 depletion (Fig. 3A). To determine whether huoMTOC is the main microtubule nucleator, we assessed the microtubule distribution in oocytes under the condition of huoMTOC deficiency. The asymmetrical distribution of microtubules was

drastically diminished, implying the essential role of the huoMTOC for microtubule nucleation in human oocytes (Fig. 3A). In addition, different degrees of disruption in the asymmetrical distribution of microtubules around the nuclear envelope were also observed after specific depletion of endogenous CCP110, CKAP5, or DISC1 (Fig. 3, B and C, and fig. S8). Of note, depletion of TACC3 resulted in the most severe disruption of microtubule asymmetrical distribution in most of the analyzed human GV oocytes (Fig. 3, B and C). These results indicate that the huoMTOC is essential for the asymmetrical nucleation of microtubules around the nuclear envelope and that all four proteins are indispensable for maintaining normal function of the huoMTOC, in which TACC3 presumably plays a leading role.

#### **The huoMTOC is fragmented and recruited to kinetochores for the initiation of spindle assembly in human oocytes**

Unlike the mechanism in mouse MI oocytes in which aMTOCs were aggregated on the spindle poles during spindle assembly (15), the components of the huoMTOC in human MI oocytes were localized on kinetochores. To reveal the dynamic process of huoMTOC-regulated spindle assembly, human GV oocytes were fixed for immunofluorescence at NEBD or at 2, 4, or 6 hours before NEBD. Initially, the huoMTOC appeared beneath the oocyte cortex. Slowly, the huoMTOC migrated from the cortex to the nuclear envelope of human GV oocytes (Fig. 4, A and B). The huoMTOC then expanded, and its nucleated microtubules grew rapidly during the resumption of meiosis (Fig. 4, A and C).

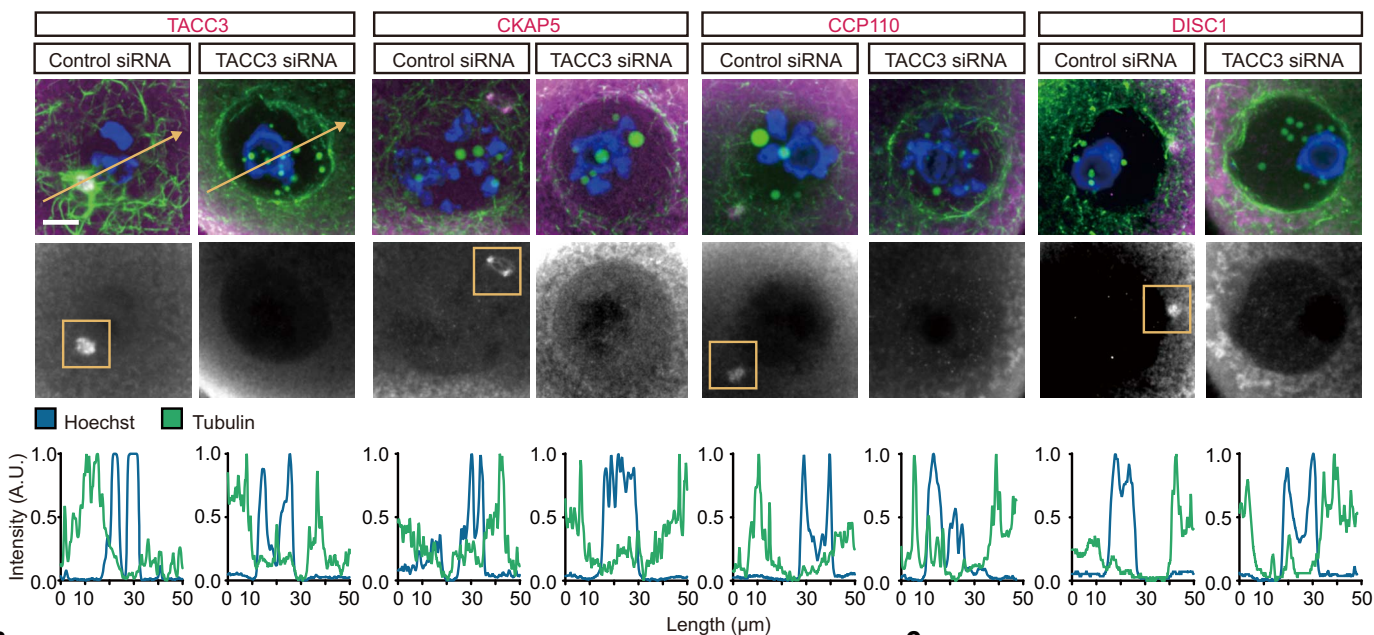
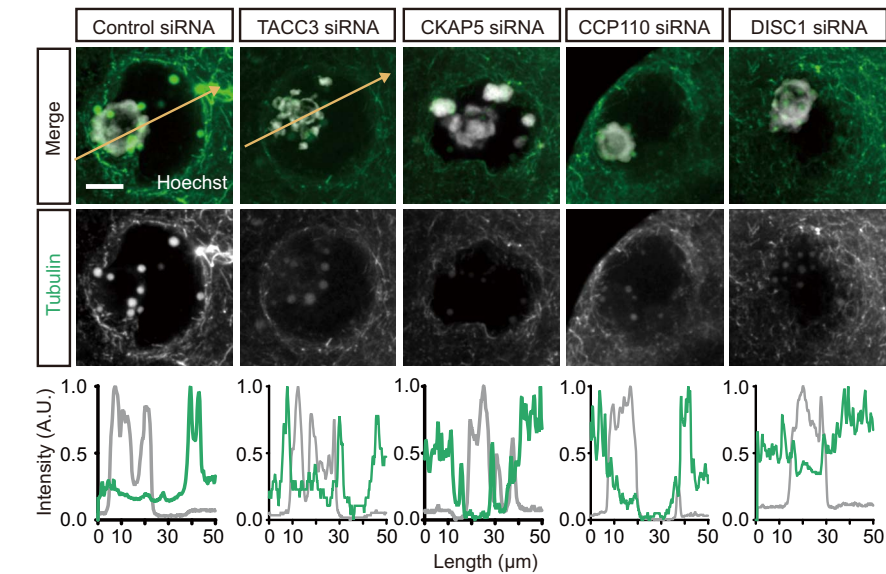
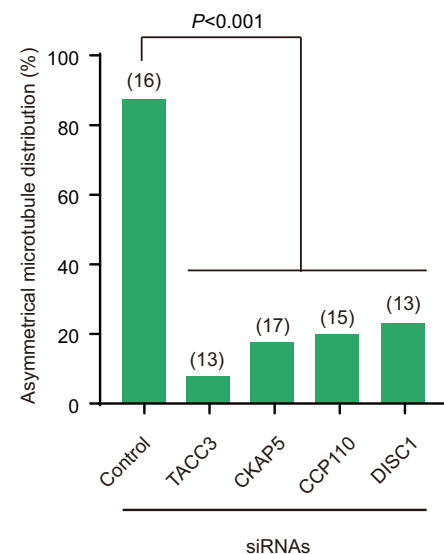
We next visualized the dynamic changes of the huoMTOC after NEBD by 3D time-lapse imaging. At the beginning of NEBD, the huoMTOC localized proximal to the chromosomes and became fragmented within the first hour (fig. S9A and movie S3). The huoMTOC microtubules were disrupted and were barely observable in the first few hours after NEBD (Fig. 4D and movie S4). The fragmented huoMTOC was then relocated to chromosomes, primarily to kinetochores (Fig. 4D, fig. S9B, and movie S5). The spindle microtubules were initially observed when the huoMTOC was rebuilt (Fig. 4, D and E; fig. S9C; and movie S4).

Next, to determine the role of the huoMTOC in spindle assembly, each huoMTOC component was down-regulated in human GV oocytes that were cultured to the MI stage. Downregulation of these components significantly impaired spindle microtubule nucleation and spindle assembly in human MI oocytes compared with the control group ( $P < 0.001$ , Fisher's exact test), and stable microtubules were greatly decreased (Fig. 4, F and G). Compared to other components, TACC3 depletion had the

most obvious effects on the microtubule nucleation and spindle assembly (Fig. 4, F and G), further suggesting that TACC3 plays a leading role in the huoMTOC. To directly test whether huoMTOC is essential for spindle assembly, the huoMTOC marked by fluorescent TACC3 was disrupted by laser ablation (fig. S10, A and B). Similar to TACC3 depletion, the spindle microtubule polymerization and spindle assembly were significantly impaired by the laser ablation of huoMTOC ( $P = 0.015$ , Fisher's exact test) (fig. S10, C and D). It has been demonstrated that RanGTP is also required for spindle assembly in human oocytes (22). Disruption of both TACC3 and RanGTP aggravated the spindle microtubule polymerization defects (fig. S11), indicating combined effects of TACC3 and RanGTP on microtubule nucleation and spindle assembly. These results suggest that the huoMTOC is required for spindle microtubule polymerization and spindle assembly of human oocytes.

#### **huoMTOC deficiency interrupts normal spindle assembly and causes clinical oocyte maturation arrest**

Oocyte maturation requires microtubule nucleation and spindle assembly (22). In the clinic, a number of infertile patients with recurrent failed in vitro fertilization (IVF) or intracytoplasmic sperm injection (ICSI) attempts have been diagnosed with oocyte maturation arrest. Considering the key role of the huoMTOC in human spindle assembly, we hypothesized that a disrupted huoMTOC resulting from mutations in *CCP110*, *CKAP5*, *DISC1*, or *TACC3* may cause impaired spindle assembly and abnormal oocyte maturation in patients. We thus screened for likely pathogenic mutations in a cohort of 1394 infertile female patients characterized by oocyte maturation arrest by analyzing their whole exome sequencing datasets (data deposited in the Genome Variation Map of the National Genomics Data Center under accession number GVM000402). Each of these patients had undergone several IVF attempts, all of which failed because of oocyte maturation arrest. We identified two patients with compound heterozygous mutations in the key huoMTOC component *TACC3* (Fig. 5A and table S1). According to the Genome Aggregation Database (gnomAD) and our in-house controls (data deposited in the Genome Variation Map of the National Genomics Data Center under accession number GVM000394), all four *TACC3* variants from patients are rare variants (table S2). Importantly, these two patients showed very similar phenotypes, in which most of their retrieved oocytes were immature after in vitro maturation (table S1), and polarization microscopy images showed no visible spindles in the live oocytes (Fig. 5B). Immunofluorescence in fixed NEBD oocytes also demonstrated that the

**A****B****C****Fig. 3. The huoMTOC is required for microtubule nucleation in human oocytes.**

**(A)** Immunofluorescence images of human GV oocytes injected with TACC3 siRNAs. Green, microtubules (tubulin); magenta, huoMTOC (yellow squares); blue, chromatin. Scale bar, 10 μm. The measurements of tubulin intensity along the direction of the yellow arrows are shown at the bottom. Green, tubulin; blue, chromosomes. **(B)** Immunofluorescence images of human GV oocytes injected with

specific siRNAs. Green, microtubules (tubulin); gray, chromosomes (Hoechst). The yellow arrows indicate the direction of the tubulin intensity measurements shown at the bottom. Scale bar, 10 μm. **(C)** The percentages of human oocytes with asymmetrical microtubule distribution in (B).  $P < 0.001$ , Fisher's exact test. Data were from three independent experiments. The number of oocytes analyzed is specified in parentheses.

meiotic spindle was completely disrupted (Fig. 5C). We also determined the stability of the huoMTOC and microtubule distribution in the patients' GV oocytes. Compared to normal human GV oocytes, the huoMTOC was missing, and the asymmetrical distribution of microtubules around the nucleus was impaired in the patients' GV oocytes (Fig. 5D).

In addition, supplementing the wild-type *TACC3* mRNA successfully rescued the phenotype of spindle disruption resulting from *TACC3*

depletion, whereas supplementing the mutant *TACC3* mRNAs could not rescue the phenotype (Fig. 5, E and F), suggesting that the mutations had loss-of-function effects on *TACC3*. Thus, *TACC3* deficiency caused female infertility and oocyte maturation arrest by disrupting the integrity of the huoMTOC. These results suggest that disruption of the huoMTOC impaired the nucleation of microtubules in the GV oocytes of patients, further highlighting the critical role of the huoMTOC in regulating microtu-

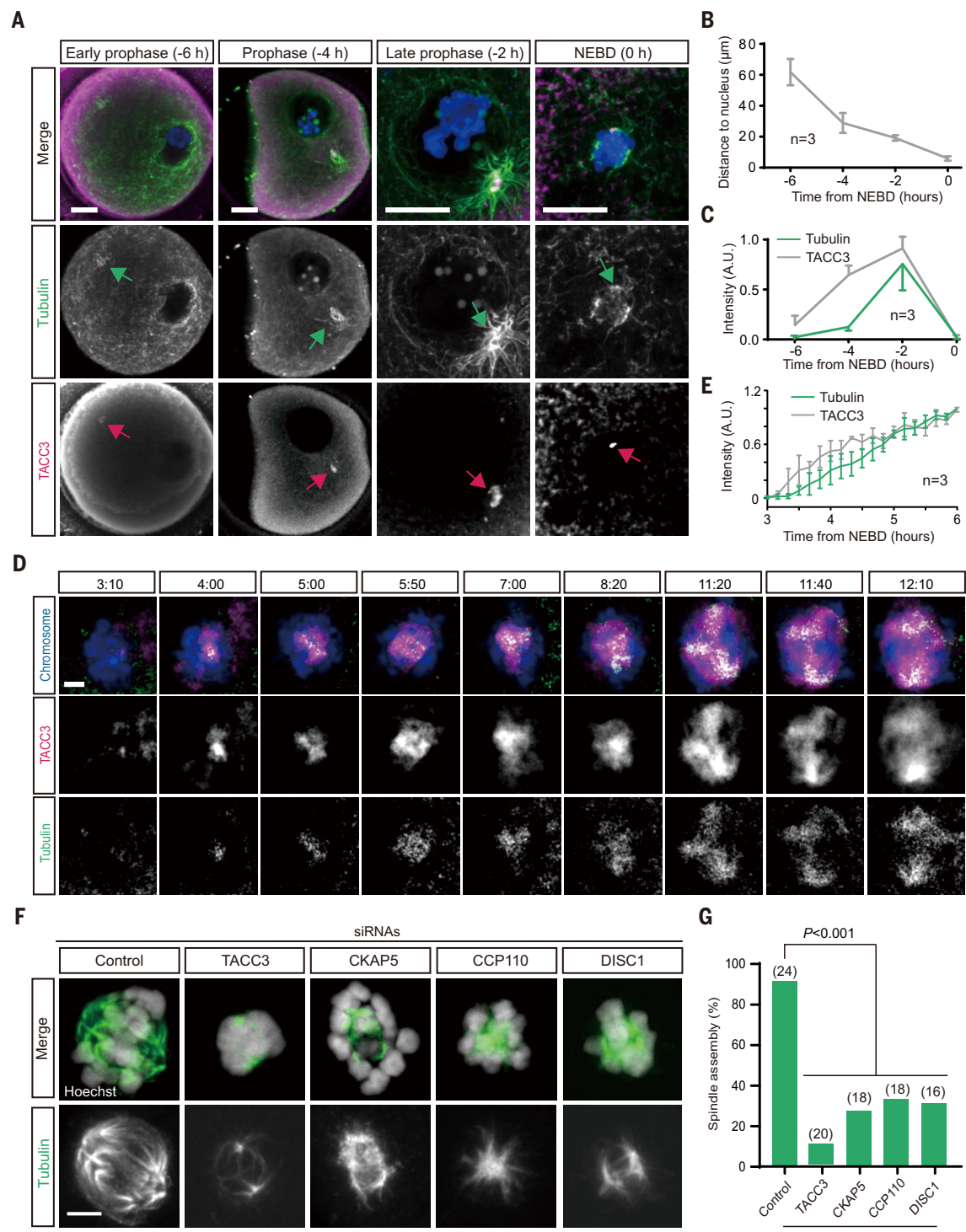
bule nucleation and the initiation of acentromosomal spindle assembly.

## Discussion

Here, we report a structure that we named the huoMTOC, which serves as a major site of microtubule nucleation and is required for spindle assembly in human oocytes. A single huoMTOC is formed near the cortex of human GV oocytes at the time of meiosis resumption, and it migrates to the nuclear envelope before

**Fig. 4. The huoMTOC is recruited from the cortex to kinetochores for spindle microtubule polymerization in human oocytes.**

(A) Immunofluorescence images of human GV oocytes at NEBD and at 2 hours (late prophase), 4 hours (prophase), and 6 hours (early prophase) before NEBD. Green, microtubules (tubulin); blue, chromatin (Hoechst); magenta, huoMTOC (TACC3). Green arrows indicate the microtubule cluster, and magenta arrows indicate the huoMTOC. Scale bar, 20  $\mu$ m. (B) The distance between the huoMTOC and the nucleus was measured in (A). Time is after NEBD. (C) The intensity of the microtubule cluster (tubulin) and the huoMTOC (TACC3) was measured at different time points in (A). Time is after NEBD. (D) Representative time-lapse images showing the relationship between the huoMTOC and microtubule nucleation in live human oocytes. Green, microtubules (SiR-tubulin); blue, chromosomes (H2B-mClover); magenta, huoMTOC (mScarlet-TACC3). Scale bar, 5  $\mu$ m. (E) The intensity of microtubules (SiR-tubulin) and huoMTOC (mClover-TACC3) close to chromosomes was measured in (D). Time is after NEBD. The number of oocytes analyzed in experiments is indicated. The mean and standard error were calculated on the basis of two independent experiments. Error bars are standard deviations. (F) Immunofluorescence images of human MI spindles from control and TACC3, CKAP5, CCP110, and DISC1 siRNA-injected human oocytes. Green, microtubules (tubulin); gray, chromosomes (Hoechst). Scale bar, 5  $\mu$ m. (G) The spindle assembly percentage measured and collected from (F). The number of oocytes analyzed in three independent experiments is indicated.  $P < 0.001$ , Fisher's exact test.



NEBD. After NEBD, the huoMTOC becomes fragmented and is recruited to chromosomes and kinetochores for spindle microtubule nucleation (Fig. 6). With the microtubule polymerization, the huoMTOC proteins are also

recruited to the spindle microtubules (Fig. 6 and fig. S9C). Ablation of the huoMTOC results in microtubule loss and defective spindle assembly. In addition, we demonstrated that TACC3, CCP110, CKAP5, and DISC1 are essential

components of the huoMTOC and that mutations in *TACC3* cause clinical oocyte maturation arrest and female infertility.

Distinct aMTOCs have been identified and investigated in mouse oocytes as microtubule

**Fig. 5. Disruption of the huoMTOC in human oocytes impairs microtubule nucleation and spindle assembly.**

(A) Pedigrees of the two families with *TACC3* mutations with Sanger sequencing confirmation. Squares denote male family members, circles denote female members, black solid circles denote probands, and the equal sign denotes infertility.

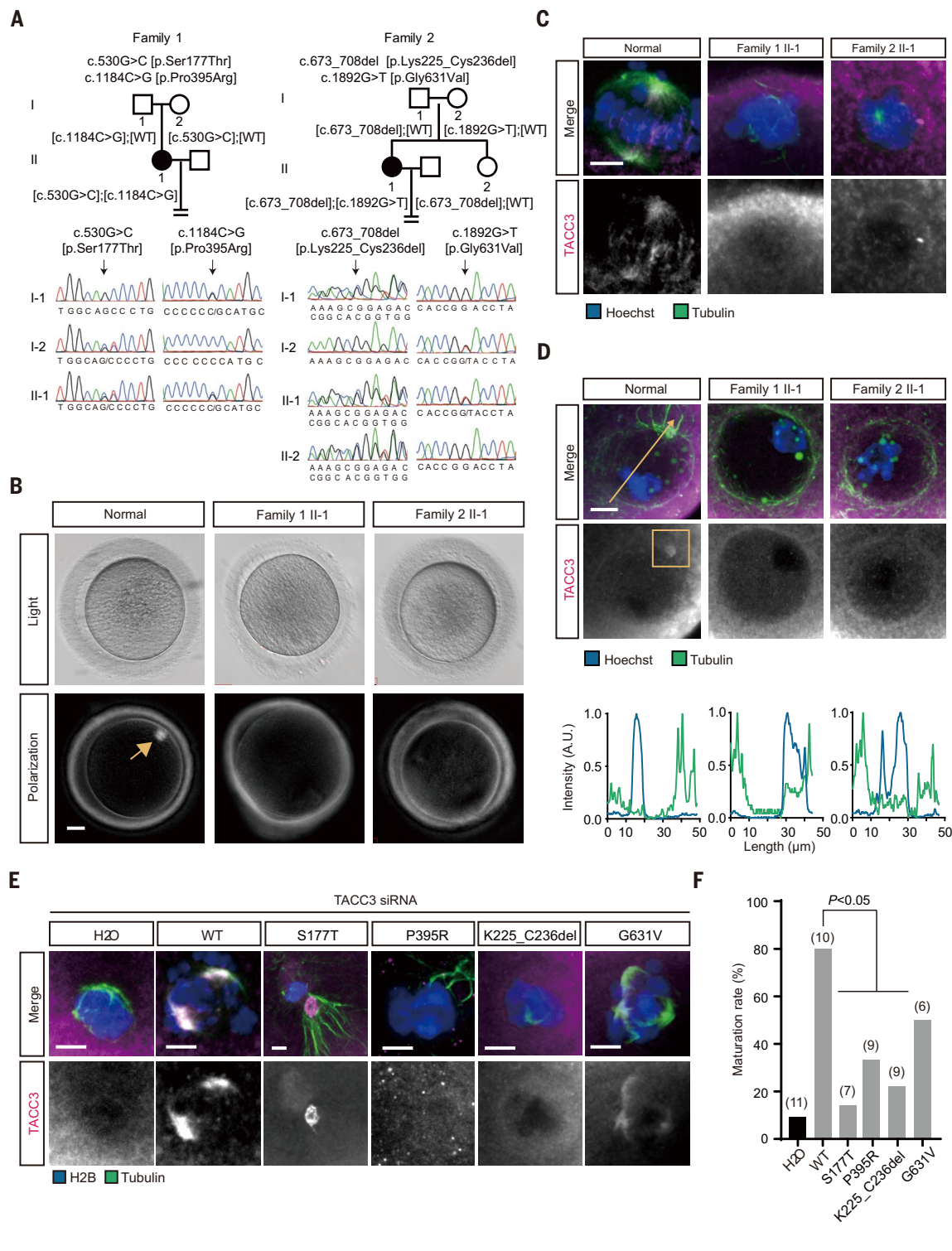
(B) Human oocytes from donors (normal) and patients (family 1 II-1, family 2 II-1) were examined by light and polarization microscopy. The arrow indicates an MI spindle. (C) Immunofluorescence images of human MI oocytes from donors (normal) and patients (family 1 II-1, family 2 II-1). Green, microtubules (tubulin); blue, chromosomes (Hoechst); magenta, TACC3. Scale bar, 5 μm.

(D) Immunofluorescence images of human GV oocytes from donors (normal) and patients (family1 II-1, family2 II-1). Green, microtubules (tubulin); blue, chromosomes (Hoechst); magenta, TACC3. Scale bar, 10 μm. The yellow square shows the huoMTOC in normal human oocyte. The microtubule distribution was measured as previously described.

(E) Immunofluorescence images of human MI oocytes injected with *TACC3* siRNAs and wild type or patient-derived mutant mRNAs. Green,

microtubules (tubulin); blue, chromosomes (Hoechst), magenta, FLAG-TACC3. Scale bar, 5 μm.

(F) The percentage of human oocyte maturation measured in (E). (Fisher's exact test,  $P < 0.05$ ). The number of oocytes analyzed is specified in parentheses.



nucleators for meiotic spindle assembly (15). However, the primary spindle microtubule nucleator of human oocytes has remained unknown. The following factors might be reasons why the huoMTOC was not identified in previous investigations: (i) Unlike mouse aMTOCs,

the huoMTOC is not concentrated on the spindle poles in human MI and MII oocytes (22). (ii) The classic aMTOC marker pericentrin is not among the components of the huoMTOC and therefore cannot label the structure. (iii) Only a single huoMTOC is formed in late prophase,

and it is fragmented immediately after NEBD, making it difficult to capture in human oocytes by immunofluorescence.

In previous investigations, spindle assembly of human oocytes was reported to be mediated by chromosomes and dependent on

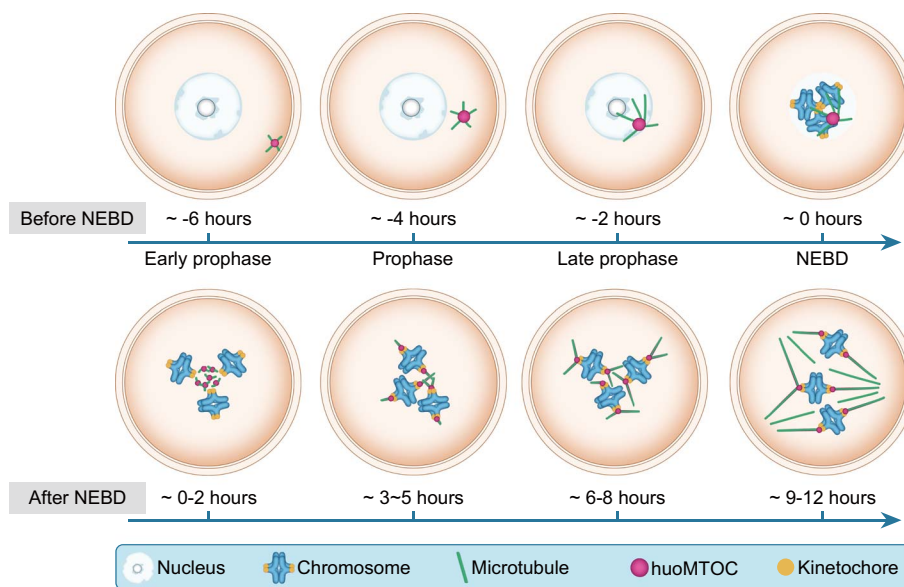


**Fig. 6. Mechanistic model for huoMTOC migration and microtubule nucleation in human oocytes.** The huoMTOC (magenta) assembles near the cortex of GV oocytes and migrates to the nuclear envelope before NEBD. The huoMTOC expands and the surrounding microtubules (green) keep growing until NEBD. After NEBD, the huoMTOC fragments, and the surrounding microtubules are disassembled. The fragmented huoMTOC is then recruited to kinetochores and initiates microtubule nucleation for meiotic spindle assembly.

RanGTP (22). It has been demonstrated that RanGTP inhibition impairs spindle assembly in human oocytes (22). In mouse or *Drosophila* oocytes, spindles have defects but still assemble if RanGTP is inhibited, suggesting that the RanGTP pathway is not essential for meiotic spindle assembly in oocytes of these two species (35, 36). In the mouse oocytes lacking centrosomes, the processes of spindle assembly and spindle microtubule nucleation are mainly achieved by aMTOCs and facilitated by liquid-like meiotic spindle domain (21, 37). It has been argued for a long time that, unlike mouse oocytes, human oocytes lack prominent aMTOCs (2, 22, 38). However, in the present study, the spindle microtubule in human oocytes was observed to be primarily polymerized from the kinetochores by an aMTOC-like structure that we named huoMTOC. In the *Drosophila* oocytes that also lack prominent aMTOCs, the spindle assembly is dominated by the chromosomes, which recruit and/or nucleate the microtubules (39). The spindle microtubules are organized around the chromosomes into fibers of two types, the interpolar and kinetochore microtubules, to assemble the meiotic spindle of *Drosophila* (39). Although the spindle assembly is directed by chromosomes in both human and *Drosophila* oocytes, the mechanisms involved could be different. The meiotic spindle assembly in *Drosophila* oocytes requires the chromosomal passenger complex (16), but that in human oocytes requires the huoMTOC.

In our study, the localization of 86 centrosome and spindle-related proteins was per-

formed in human MI oocytes by systematic immunofluorescent staining. We identified the components (TACC3, CKAP5, CCP110, and DISC1) of the huoMTOC on kinetochores in MI oocytes and then verified their localization in GV oocytes using high-resolution imaging in live human oocytes. Emerging evidence suggests that the human TACC3 plays an important role in microtubule growth and spindle assembly during mitosis (30, 40–42). The microtubule nucleation is blocked in ovarian cancer cells when TACC3 expression is affected, suggesting that TACC3 is required for centrosome-involved microtubule nucleation (43). TACC3 depletion impairs the  $\gamma$ -tubulin ring complex assembly (44) and centrosome integrity (45) of human somatic cells. CKAP5 was previously identified as a microtubule nucleation factor in vitro (32, 33, 46). CKAP5 was observed functioning synergistically with the  $\gamma$ -tubulin ring complex for de novo microtubule nucleation (32) and catalyzing numerous rounds of tubulin subunit addition at the microtubule plus-end for spindle microtubule assembly in vitro (33). In addition, CKAP5 was also implicated in the importin-regulated microtubule nucleation as a microtubule polymerase in vitro (46). In mitosis, TACC3 and CKAP5 are RanGTP-regulated spindle assembly factors for spindle microtubule nucleation and stabilization (47–49). Collectively, we inferred that TACC3 and CKAP5 may act as organizers of huoMTOC assembly and microtubule nucleation in human oocytes. The functions of CCP110 and DISC1 in micro-

tubule polymerization have not yet been determined in either mitotic or meiotic cells.

Apart from the four huoMTOC components, we also identified 39 other proteins that showed spindle-related localization. We therefore cannot exclude the possibility that some of these proteins may also play a role in huoMTOC formation and function. The specific components of huoMTOC and the mechanism for its nucleation of microtubules are worth investigating in the future. In addition, according to our observations, the localization of most centrosome and microtubule-related proteins in the MI spindle of human oocytes is obviously different from that in mouse oocytes (21). Thus, future investigations on the functions of these proteins in human oocytes should shed more light on the mechanism of human oocyte spindle assembly.

In a recent study, a distinct mechanism of spindle pole organization was discovered in human oocytes, suggesting that loss of kinesin superfamily protein C1 (KIFC1) induces meiotic spindle instability (23). In addition, our previous investigations suggest that tubulin beta 8 class VIII (TUBB8) is the main isotype of spindle  $\beta$ -tubulin in human oocytes but is not found in mice or other nonprimate species (50). These findings suggest that a distinct mechanism for the initiation of microtubule nucleation and spindle assembly has evolved in human oocytes, which may contribute to a series of physiological characteristics including increasing chromosome segregation errors, high spindle instability, and aneuploidy in human oocytes.

In the clinic, many infertility patients experience recurrent failure of IVF or ICSI attempts owing to oocyte maturation arrest. However, the genetic factors involved remain unknown for most patients. In this study, we found that mutations in TACC3 cause defects in spindle assembly by disrupting the structure of the huoMTOC, which leads to oocyte maturation arrest in patients. It is worth performing mutational screening for both known and potential genes that might participate in the maintenance of huoMTOC integrity. The results of such screening will help in precision diagnosis for these patients and will provide therapeutic targets for future clinical treatments. Our findings provide not only insights into the physiological mechanism of microtubule nucleation and spindle assembly in human oocytes but also improve our understanding of pathophysiological mechanisms of human oocyte maturation arrest.

## Materials and methods

### Human oocyte collection and culture

Human GV oocytes were donated by patients undergoing ICSI as part of their assisted reproduction treatment at Shanghai Ji Ai Genetics and IVF Institute affiliated with the Obstetrics and Gynecology Hospital of Fudan University,

Center for Reproductive Medicine and Fertility Preservation program affiliated with International Peace Maternity and Child Health Hospital of Shanghai Jiao Tong University. Only immature oocytes that were unable to be used for assisted reproduction treatment were collected for this research, and the use of these human GV oocytes was clearly explained to the patient donors. All these female donors were receiving ICSI treatment because of male factor-induced infertility. The age range of the donors was 25 to 38 and their mean age was 34.3. The BMI range of these donors was 20 to 22. The collected human oocytes were mixed thoroughly and distributed randomly to the control and experimental groups. Only morphologically normal human GV oocytes were used in this investigation. G-MOPS medium (Vitrolife) with milrinone (2  $\mu$ M, HY-14252, MedChemExpress) was used to maintain human oocyte prophase arrest. The human GV oocytes were matured in Multipurpose Handling Medium-Complete (MHM-C) (FUJIFILM Irvine Scientific) or G-MOPS medium at 37°C on a heating block.

#### Animals and oocyte culture

The porcine ovaries were collected from local slaughterhouses and transported in warm 0.9% NaCl. Porcine GV oocytes were collected in TCM199 medium at 39°C, and milrinone (2  $\mu$ M) was added to the medium to maintain oocyte prophase arrest. Only fully grown oocytes were used in our experiments. For maturation, GV oocytes were washed free from milrinone and cultured in fresh TCM199 medium at 39°C and 5% CO<sub>2</sub>. Porcine GV and MI oocytes were fixed for immunofluorescence at 6 or 15 hours after oocyte isolation, respectively.

Female C57Bl/6 mice (3- to 4-week-old) were purchased from Beijing Vital River Laboratory Animal Technology Co., Ltd. (Beijing, China). All mice were used in accordance with institutional guidelines, and the experiments were approved by the Animal Care and Use Committee of Fudan University, China. Mouse GV oocytes were released from the ovaries at 44 to 52 hours after injection of 10 IU pregnant mare serum gonadotropin. For maturation, denuded GV oocytes were cultured in fresh M2 medium at 37°C on a heat block. The pH value of culture medium was between 7.2 and 7.4 (S210, Mettler Toledo). Mouse GV and MI oocytes were fixed for immunofluorescence at 0.5 or 6 hours after in vitro maturation initiation, respectively.

#### Inhibitor treatment

For microtubule depolymerization, nocodazole (10  $\mu$ M, HY-13520, MedChemExpress) was added to human oocytes at ~10 hours after NEBD and 1 hour before time-lapse imaging. The drug was dissolved in dimethyl sulfoxide

(Sigma-Aldrich) and used at a concentration of 0.1% in G-MOPS.

#### Immunofluorescence microscopy

Human GV oocytes were fixed for immunofluorescence at 2, 4, or 6 hours after milrinone washout. Human MI oocytes were fixed at 5 to 12 hours after NEBD (prometaphase or metaphase). Human oocytes were fixed for 30 min in phosphate-buffered saline (PBS) containing 2% formaldehyde and 0.1% Triton-X at 37°C on a heat block and were then permeabilized in PBS containing 0.5% Triton-X (PBT) at 4°C overnight. Oocytes were extensively washed with PBS between stages and then blocked at room temperature in a blocking buffer of 3% bovine serum albumin (BSA) in 0.3% PBT. All antibody incubations were performed in blocking buffer at 4°C overnight for primary antibodies and at 37°C for 1 hour for secondary antibodies. Primary antibodies were anti-centromere antibody (HCT-0100; ImmunoVision; 1:500), anti-AKAP450 antibody (611518; BD Biosciences; 1:50), anti-ASPM antibody (26223-1-AP; Proteintech; 1:50), anti-AURKA antibody (NBP2-50041; Novus Biological; 1:50), anti-AURKA antibody (10297-1-AP; Proteintech; 1:20), anti-AURKB antibody (ab45145; Abcam; 1:50), anti-BBS4 antibody (12766-1-AP; Proteintech; 1:50), anti-beta tubulin antibody (ab204686; Abcam; 1:50), anti-beta tubulin antibody (ab11309; Abcam; 1:100), anti-BUGZ antibody (A20177; ABclonal; 1:20), anti-CAMSAP2 antibody (17880-1-AP; Proteintech; 1:50), anti-CCP110 antibody (12780-1-AP; Proteintech; 1:50), anti-CCP110 antibody (PA5-58775; Thermo Fisher Scientific; 1:100), anti-CDK5RAP2 antibody (06-1398; Merck; 1:100), anti-CENPJ antibody (I1517-1-AP; Proteintech; 1:50), anti-CEP57 antibody (24957-1-AP; Proteintech; 1:50), anti-CEP63 antibody (16268-1-AP; Proteintech; 1:50), anti-CEP72 antibody (19928-1-AP; Proteintech; 1:50), anti-CEP120 antibody (PA5-55985; Thermo Fisher Scientific; 1:100), anti-CEP135 antibody (24428-1-AP; Proteintech; 1:50), anti-CEP152 antibody (21815-1-AP; Proteintech; 1:50), anti-CEP164 antibody (22227-1-AP; Proteintech; 1:50), anti-CEP170 antibody (27325-1-AP; Proteintech; 1:50), anti-CEP192 antibody (18832-1-AP; Proteintech; 1:50), anti-CEP250 antibody (I4498-1-AP; Proteintech; 1:50), anti-CEP290 antibody (22490-1-AP; Proteintech; 1:50), anti-CETN2 antibody (A5397; ABclonal; 1:20), anti-CETN3 antibody (A8111; ABclonal; 1:50), anti-CKAP5 antibody (PA5-59150; Thermo Fisher Scientific; 1:100), anti-CKAP5 antibody (CL488-67631; Proteintech; 1:50), anti-CLIP1 antibody (23839-1-AP; Proteintech; 1:50), anti-CLTC antibody (610500; BD Biosciences; 1:50), anti-CNTROB antibody (26880-1-AP; Proteintech; 1:50), anti-DCTN1 antibody (55182-1-AP; Proteintech; 1:50), anti-DCTN2 antibody (A2200; ABclonal; 1:50), anti-DYNC1HI antibody (I2345-1-AP; Proteintech; 1:50), anti-DISC1 antibody (A4678; ABclonal;

1:50), anti-DLGAP5 antibody (A13575; ABclonal; 1:50), anti-DYNLT1 antibody (11954-1-AP; Proteintech; 1:50), anti-GTSE1 antibody (A302-425A; Bethyl Laboratories; 1:50), anti-HAUS4 antibody (20104-1-AP; Proteintech; 1:50), anti-HAUS6 antibody (A4797; ABclonal; 1:50), anti-HAUS8 antibody (PA5-21331; Thermo Fisher Scientific; 1:100), anti-HMMR antibody (15820-1-AP; Proteintech; 1:50), anti-HOOK2 antibody (ab133691; Abcam; 1:50), anti-HOOK3 antibody (A15536; ABclonal; 1:50), anti-HOOK3 antibody (15457-1-AP; Proteintech; 1:50), anti-KANSL3 antibody (HPA035018; Merck; 1:100), anti-KIF11 antibody (HPA010568; Merck; 1:100), anti-KIF20A antibody (15911-1-AP; Proteintech; 1:50), anti-KIF20A antibody (CL594-67190; Proteintech; 1:50), anti-KIF22 antibody (A19881; ABclonal; 1:50), anti-KIF2A antibody (13105-1-AP; Proteintech; 1:50), anti-KIF2B antibody (A6480; ABclonal; 1:20), anti-KIFC1 antibody (A3304; ABclonal; 1:20), anti-KIZ antibody (21177-1-AP; Proteintech; 1:50), anti-LIS1 antibody (H00005048-M03; Abnova; 1:50), anti-LMNB antibody (A1910; ABclonal; 1:20), anti-LRRC45 antibody (PA5-54777; Thermo Fisher Scientific; 1:100), anti-MCRS1 antibody (HPA039057; Merck; 1:100), anti-MYO10 antibody (sc-23137; SantaCruz Biotechnology; 1:50), anti-NDEL1 antibody (10233-1-AP; Proteintech; 1:50), anti-NDEL1 antibody (H00081565-D01P; Abnova; 1:50), anti-NEDD1 antibody (13993-1-AP; Proteintech; 1:50), anti-NEK2 antibody (14233-1-AP; Proteintech; 1:50), anti-NIN antibody (A8215; ABclonal; 1:50), anti-NUMA1 antibody (A0527; ABclonal; 1:50), anti-NUP107 antibody (A13110; ABclonal; 1:50), anti-NUP160 antibody (PR54707; Merck; 1:100), anti-NUP62 antibody (13916-1-AP; Proteintech; 1:50), anti-NUP85 antibody (19370-1-AP; Proteintech; 1:50), anti-NUSAP1 antibody (I2024-1-AP; Proteintech; 1:50), anti-ODF2 antibody (I2058-1-AP; Proteintech; 1:50), anti-PCNT antibody (611815; BD Biosciences; 1:200), anti-PCM1 antibody (19856-1-AP; Proteintech; 1:50), anti-PLK1 antibody (A2548; ABclonal; 1:50), anti-PLK3 antibody (10977-1-AP; Proteintech; 1:50), anti-PLK4 antibody (12952-1-AP; Proteintech; 1:50), anti-PRC1 antibody (15617-1-AP; Proteintech; 1:50), anti-RAE1 antibody (20491-1-AP; Proteintech; 1:50), anti-RAN antibody (10469-1-AP; Proteintech; 1:50), anti-SASS6 antibody (21377-1-AP; Proteintech; 1:50), anti-SKAP2 antibody (12926-1-AP; Proteintech; 1:50), anti-SNF2H antibody (A2000; ABclonal; 1:50), anti-SPDL1 antibody (PA5-99285; Thermo Fisher Scientific; 1:100), anti-SSX2IP antibody (13694-1-AP; Proteintech; 1:50), anti-TACC3 antibody (A18641; ABclonal; 1:50), anti-TACC3 antibody (ab134154; Abcam; 1:100), anti-TOP2A antibody (20233-1-AP; Proteintech; 1:50), anti-TPX2 antibody (A18327; ABclonal; 1:20), anti-TUBG1 antibody (A9657; ABclonal; 1:20). Secondary antibodies were Alexa Fluor 647-conjugated anti-rabbit IgG (4414S; Cell Signaling; 1:200), Alexa Fluor 647-conjugated

anti-mouse IgG (4410S; Cell Signaling; 1:200), Cy3-conjugated anti-rabbit IgG (AS008; Abclonal; 1:500), and Atto 488-conjugated anti-human IgG (52526; Merck; 1:500). Chromatin was briefly counterstained with Hoechst 33342 (20  $\mu\text{g}\cdot\text{ml}^{-1}$ , HY-15559, MedChemExpress) before imaging. The samples were in PBS and imaged with an LSM 880 confocal laser scanning microscope (ZEISS) with a  $63\times/1.4$  NA Plan Apochromat oil immersion lens at room temperature.

#### RNA interference

The siRNAs were provided by GenePharma or Tsingke Biotechnology. The sequences of siRNA for TACC3 down-regulation were 5'-GGU UCG AAG AGG UUG UGU A-3' and 5'-GCA UGC ACG GUG CAA AUG A-3'. The siRNA sequences against CKAP5 were 5'-GGA AAT AGC TGT TCA CAT A-3' and 5'-GGC CAA AGC TCC AGG ATT A-3'. The siRNA sequences targeting CCP110 were 5'-CAC UCU ACU GCA GCA AAG C-3' and 5'-AUG UUC UUC UCC AAG GUG C-3'. The siRNA sequence targeting DISC1 was 5'-GGA UUU GAG AAU AGU UUC A-3'. The negative control siRNAs were provided by the same company. To increase the efficiency of RNA inhibition, mixed siRNAs were microinjected into human GV oocytes. The final concentration of siRNAs was 40  $\mu\text{M}$ .

#### Microinjection of human oocytes

Human GV oocytes were microinjected in G-MOPS with milrinone (2  $\mu\text{M}$ ) on the stage of an inverted microscope (Leica) with micromanipulators (Eppendorf). A 0.1 to 0.3% volume of mRNA was injected using a timed pulse, and the final concentration of mRNA was 1  $\mu\text{g}/\mu\text{l}$ . The injected GV oocytes were arrested in prophase for 2–4 hours for mRNA expression.

#### mRNA synthesis

mRNA was transcribed in vitro from purified linear double-stranded DNA templates. mMessage T7 or T3 RNA polymerase kits (New England Biolabs) were used for the in vitro transcription reaction. The constructs of mClover3-CENPB, mScarlet-CENPB, mClover3-TACC3, mScarlet-TACC3, mClover3-CKAP5, mClover3-CCP110, and mClover3-DISC1 were made and used for mRNA production.

#### Live cell imaging

For high-resolution time-lapse imaging, time points were acquired at 10-min intervals using an LSM 880 confocal laser scanning microscope (ZEISS) fitted with sensitive detectors, an environmental chamber set to 37°C, and a long-distance  $40\times/1.1$  NA C-Apochromat water immersion lens. A volume of 30  $\mu\text{m}$  by 30  $\mu\text{m}$  by 15  $\mu\text{m}$  centered around the chromosomes was typically imaged. The chromosomes were tracked automatically by MyPiC on LSM880. Microtubules in live human oocytes were

visualized by SiR-tubulin (1  $\mu\text{M}$ ) staining in G-MOPS. To reduce background noise, some images were passed through a Gaussian filter of 2 sigma in Fiji (NIH).

#### Fluorescent intensity measurement

The pattern of microtubule distribution was defined by the intensity of tubulin around the nuclear envelope. The direction of intensity measurements is shown in the figures. The intensity was measured by Image J (NIH). The integrated intensity of kinetochore foci was measured with the Foci\_Picker3D plugin in Image J. The same threshold was applied to each focus within an oocyte.

#### Laser ablation

To examine the role of huoMTOC in microtubule polymerization of human oocytes, the huoMTOC was directly disrupted by laser in live human GV oocytes. The human GV oocytes expressing mClover3-TACC3 were rotated with an unbroken microinjection pipette to obtain huoMTOC. The square regions of interest were marked and photobleached using a 488-nm laser line at the maximum power. The laser ablation was performed at 37°C.

#### Cell culture and transfection

HEK293T cells were obtained from the Cell Bank of Shanghai Institute for Biological Sciences, the Chinese Academy of Sciences (Shanghai, China). Cells were cultured in Dulbecco's modified Eagle's medium supplemented with 10% fetal bovine serum and 1% penicillin-streptomycin (Gibco, Waltham, MA, USA) in an atmosphere of 5% CO<sub>2</sub> at 37°C to between 70 and 80% confluence. Plasmids were transfected into HEK293T cells using the PolyJet In Vitro DNA Transfection Reagent (SigmaGen) according to the manufacturer's instructions.

#### Immunoblots and immunoprecipitation

HEK293T cells were harvested after transfection for 36 hours and washed with PBS. Cells were lysed in radioimmunoprecipitation assay lysis buffer (Shanghai Wei AO Biological Technology, Shanghai, China) with 1% protease inhibitor cocktail (Bimake, Houston, TX, USA). After quantification with the bicinchoninic acid assay (Shanghai Biocolor BioScience & Technology Co.), the supernatant was subjected to immunoprecipitation with affinity beads (Sigma). After incubation at 4°C for 4 hours, the beads were washed with lysis buffer four times.

The bead-bound proteins were eluted using sodium dodecyl sulfate (SDS) sample buffer, resolved by SDS-polyacrylamide gel electrophoresis (SDS-PAGE), transferred to nitrocellulose membranes (Pall Corporation), and probed with rabbit anti-FLAG (1:3000 dilution; Cell Signaling Technology) or mouse anti-vinculin (1:5000 dilution; Sigma-Aldrich) antibodies. The secondary antibodies were goat anti-rabbit

immunoglobulin G (IgG) (1:5000 dilution; Abmart) or goat anti-mouse IgG (1:5000 dilution; Abmart) conjugated to horseradish peroxidase.

#### Clinical samples

A cohort of 1394 infertile female patients with oocyte maturation arrest recruited from the Ninth Hospital affiliated with Shanghai Jiao Tong University and Shanghai Ji Ai Genetics and IVF Institute affiliated with the Obstetrics and Gynecology Hospital of Fudan University participated in this study. Written informed consent was provided by patients. The recruitment of patients was performed as follows: (i) female patients were younger than 45 years old, failing to conceive after 1 year (or longer) of regular unprotected sex; (ii) had undergone  $\geq 2$  failed attempts of IVF/ICSI, characterized by oocyte maturation arrest; (iii) female patients with other known causes of infertility, including male factors, chromosome anomalies, radiotherapy, or chemotherapy, were excluded. Peripheral blood samples were taken for DNA extraction.

The GV and MI oocytes from two patients with compound heterozygous mutations in TACC3 were obtained as part of their assisted reproduction treatment at the Shanghai Ninth Hospital affiliated to Shanghai Jiao Tong University.

This study was approved by the Ethics Committee of the Medical College of Fudan University and the Reproductive Study Ethics Committees of the hospitals.

#### Genetic studies

Genomic DNA was extracted from peripheral blood using the QIAamp DNA Blood Mini Kit (Qiagen). Whole-exome capture was performed using the SeqCap EZ Exome Kit (Roche), and sequencing was performed on the Illumina NovaSeq 6000 platform (Illumina). Sequencing analysis was compared with the human reference sequence (NCBI Genome build GRCh37). Mutations were annotated with GRCh37 and the dbSNP (version 138) and gnomAD along with our in-house exome database (data deposited in public database, accession numbers GVM000402 and GVM000394).

#### Statistical analysis

The investigators were not blinded during experiments and outcome assessment. The experiments were not randomized. The statistical methods were not used to determine sample size. Sample means were compared with either Student's *t* test or one-way analysis of variance (ANOVA) with a post-hoc test as stated (two-sided). Dichotomous data were compared using Fisher's exact test (two-tailed). All data are from at least two independent experiments. All tests were performed using GraphPad Prism 7 (GraphPad Software).

## REFERENCES AND NOTES

1. S. L. Prosser, L. Pelletier, Mitotic spindle assembly in animal cells: A fine balancing act. *Nat. Rev. Mol. Cell Biol.* **18**, 187–201 (2017). doi: [10.1038/nrm.2016.162](https://doi.org/10.1038/nrm.2016.162); pmid: [28174430](https://pubmed.ncbi.nlm.nih.gov/28174430/)
2. B. Mogessie, K. Scheffler, M. Schuh, Assembly and positioning of the oocyte meiotic spindle. *Annu. Rev. Cell Dev. Biol.* **34**, 381–403 (2018). doi: [10.1146/annurev-cellbio-100616-060553](https://doi.org/10.1146/annurev-cellbio-100616-060553); pmid: [30028643](https://pubmed.ncbi.nlm.nih.gov/30028643/)
3. S. Doxsey, Re-evaluating centrosome function. *Nat. Rev. Mol. Cell Biol.* **2**, 688–698 (2001). doi: [10.1038/35089575](https://doi.org/10.1038/35089575); pmid: [11533726](https://pubmed.ncbi.nlm.nih.gov/11533726/)
4. S. Petry, Mechanisms of mitotic spindle assembly. *Annu. Rev. Biochem.* **85**, 659–683 (2016). doi: [10.1146/annurev-biochem-060815-014528](https://doi.org/10.1146/annurev-biochem-060815-014528); pmid: [27154846](https://pubmed.ncbi.nlm.nih.gov/27154846/)
5. A. Verti, H. Hehnly, S. Doxsey, The centrosome, a multitalented renaissance organelle. *Cold Spring Harb. Perspect. Biol.* **8**, a025049 (2016). doi: [10.1101/cshperspect.a025049](https://doi.org/10.1101/cshperspect.a025049); pmid: [27098937](https://pubmed.ncbi.nlm.nih.gov/27098937/)
6. J. L. Badano, T. M. Teslovich, N. Katsanis, The centrosome in human genetic disease. *Nat. Rev. Genet.* **6**, 194–205 (2005). doi: [10.1038/ng1557](https://doi.org/10.1038/ng1557); pmid: [15738963](https://pubmed.ncbi.nlm.nih.gov/15738963/)
7. D. Szollosi, P. Calarco, R. P. Donahue, Absence of centrioles in the first and second meiotic spindles of mouse oocytes. *J. Cell Sci.* **11**, 521–541 (1972). doi: [10.1242/jcs.11.2.521](https://doi.org/10.1242/jcs.11.2.521); pmid: [5076360](https://pubmed.ncbi.nlm.nih.gov/5076360/)
8. A. T. Hertig, E. C. Adams, Studies on the human oocyte and its follicle. I. Ultrastructural and histochemical observations on the primordial follicle stage. *J. Cell Biol.* **34**, 647–675 (1967). doi: [10.1083/jcb.34.2.647](https://doi.org/10.1083/jcb.34.2.647); pmid: [4292010](https://pubmed.ncbi.nlm.nih.gov/4292010/)
9. T. Mikeladze-Dvali *et al.*, Analysis of centriole elimination during *C. elegans* oogenesis. *Development* **139**, 1670–1679 (2012). doi: [10.1242/dev.075440](https://doi.org/10.1242/dev.075440); pmid: [22492357](https://pubmed.ncbi.nlm.nih.gov/22492357/)
10. A. Pimenta-Marques *et al.*, A mechanism for the elimination of the female gamete centrosome in *Drosophila melanogaster*. *Science* **353**, aaf4866 (2016). doi: [10.1126/science.aaf4866](https://doi.org/10.1126/science.aaf4866); pmid: [27229142](https://pubmed.ncbi.nlm.nih.gov/27229142/)
11. G. Manandhar, H. Schatten, P. Sutovsky, Centrosome reduction during gametogenesis and its significance. *Biol. Reprod.* **72**, 2–13 (2005). doi: [10.1095/biolreprod.104.031245](https://doi.org/10.1095/biolreprod.104.031245); pmid: [15385423](https://pubmed.ncbi.nlm.nih.gov/15385423/)
12. D. L. Gard, Microtubule organization during maturation of *Xenopus* oocytes: Assembly and rotation of the meiotic spindles. *Dev. Biol.* **151**, 516–530 (1992). doi: [10.1016/0012-1606\(92\)90190-R](https://doi.org/10.1016/0012-1606(92)90190-R); pmid: [1601183](https://pubmed.ncbi.nlm.nih.gov/1601183/)
13. M. Łukasz, I. Queguiner, M. H. Verhac, S. Brunet, Rebuilding MTOCs upon centriole loss during mouse oogenesis. *Dev. Biol.* **382**, 48–56 (2013). doi: [10.1016/j.ydbio.2013.07.029](https://doi.org/10.1016/j.ydbio.2013.07.029); pmid: [23954884](https://pubmed.ncbi.nlm.nih.gov/23954884/)
14. M. J. Carabatos, C. M. H. Combelles, S. M. Messinger, D. F. Albertini, Sorting and reorganization of centrosomes during oocyte maturation in the mouse. *Microsc. Res. Tech.* **49**, 435–444 (2000). doi: [10.1002/\(SICI\)1097-0029\(20000601\)49:4<435::AID-JEMT5>3.0.CO;2-H](https://doi.org/10.1002/(SICI)1097-0029(20000601)49:4<435::AID-JEMT5>3.0.CO;2-H); pmid: [10842370](https://pubmed.ncbi.nlm.nih.gov/10842370/)
15. M. Schuh, J. Ellenberg, Self-organization of MTOCs replaces centrosome function during acentrosomal spindle assembly in live mouse oocytes. *Cell* **130**, 484–498 (2007). doi: [10.1016/j.cell.2007.06.025](https://doi.org/10.1016/j.cell.2007.06.025); pmid: [17693257](https://pubmed.ncbi.nlm.nih.gov/17693257/)
16. S. J. Radford, A. L. Nguyen, K. Schindler, K. S. McKim, The chromosomal basis of meiotic acentrosomal spindle assembly and function in oocytes. *Chromosoma* **126**, 351–364 (2017). doi: [10.1007/s00412-016-0618-1](https://doi.org/10.1007/s00412-016-0618-1); pmid: [27837282](https://pubmed.ncbi.nlm.nih.gov/27837282/)
17. I. D. Wolff, M. V. Tran, T. J. Mullen, A. M. Villeneuve, S. M. Wignall, Assembly of *Caenorhabditis elegans* acentrosomal spindles occurs without evident microtubule-organizing centers and requires microtubule sorting by KLP-18/kinesin-12 and MESP-1. *Mol. Biol. Cell* **27**, 3122–3131 (2016). doi: [10.1091/mbe.e16-05-0291](https://doi.org/10.1091/mbc.e16-05-0291); pmid: [27559133](https://pubmed.ncbi.nlm.nih.gov/27559133/)
18. D. Clift, M. Schuh, A three-step MTOC fragmentation mechanism facilitates bipolar spindle assembly in mouse oocytes. *Nat. Commun.* **6**, 7217 (2015). doi: [10.1038/ncomms8217](https://doi.org/10.1038/ncomms8217); pmid: [26147444](https://pubmed.ncbi.nlm.nih.gov/26147444/)
19. T. Wu, S. I. R. Lane, S. L. Morgan, K. T. Jones, Spindle tubulin and MTOC asymmetries may explain meiotic drive in oocytes. *Nat. Commun.* **9**, 2952 (2018). doi: [10.1038/s41467-018-05338-7](https://doi.org/10.1038/s41467-018-05338-7); pmid: [30054463](https://pubmed.ncbi.nlm.nih.gov/30054463/)
20. C. Gueth-Hallonet *et al.*,  $\gamma$ -Tubulin is present in acentriolar MTOCs during early mouse development. *J. Cell Sci.* **105**, 157–166 (1993). doi: [10.1242/jcs.105.1.157](https://doi.org/10.1242/jcs.105.1.157); pmid: [8360270](https://pubmed.ncbi.nlm.nih.gov/8360270/)
21. C. So *et al.*, A liquid-like spindle domain promotes acentrosomal spindle assembly in mammalian oocytes. *Science* **364**, eaat9557 (2019). doi: [10.1126/science.aat9557](https://doi.org/10.1126/science.aat9557); pmid: [31249032](https://pubmed.ncbi.nlm.nih.gov/31249032/)
22. Z. Holubcová, M. Blayney, K. Elder, M. Schuh, Error-prone chromosome-mediated spindle assembly favors chromosome segregation defects in human oocytes. *Science* **348**, 1143–1147 (2015). doi: [10.1126/science.aaa9529](https://doi.org/10.1126/science.aaa9529); pmid: [26045437](https://pubmed.ncbi.nlm.nih.gov/26045437/)
23. C. So *et al.*, Mechanism of spindle pole organization and instability in human oocytes. *Science* **375**, eabj3944 (2022). doi: [10.1126/science.abj3944](https://doi.org/10.1126/science.abj3944); pmid: [35143306](https://pubmed.ncbi.nlm.nih.gov/35143306/)
24. T. Wu, S. I. R. Lane, S. L. Morgan, F. Tang, K. T. Jones, Loss of centromeric RNA activates the spindle assembly checkpoint in mammalian female meiosis I. *J. Cell Biol.* **220**, e202011153 (2021). doi: [10.1083/jcb.202011153](https://doi.org/10.1083/jcb.202011153); pmid: [34379093](https://pubmed.ncbi.nlm.nih.gov/34379093/)
25. J. R. A. Hutchins *et al.*, Systematic analysis of human protein complexes identifies chromosome segregation proteins. *Science* **328**, 593–599 (2010). doi: [10.1126/science.1181348](https://doi.org/10.1126/science.1181348); pmid: [20360068](https://pubmed.ncbi.nlm.nih.gov/20360068/)
26. H. V. Goodson, E. M. Jonasson, Microtubules and microtubule-associated proteins. *Cold Spring Harb. Perspect. Biol.* **10**, a022608 (2018). doi: [10.1101/cshperspect.a022608](https://doi.org/10.1101/cshperspect.a022608); pmid: [29858272](https://pubmed.ncbi.nlm.nih.gov/29858272/)
27. Z. Chen, V. B. Indjeian, M. McManus, L. Wang, B. D. Dynlach, CP110, a cell cycle-dependent CDK substrate, regulates centrosome duplication in human cells. *Dev. Cell* **3**, 339–350 (2002). doi: [10.1016/S1534-5807\(02\)00258-7](https://doi.org/10.1016/S1534-5807(02)00258-7); pmid: [12361598](https://pubmed.ncbi.nlm.nih.gov/12361598/)
28. F. Gergely *et al.*, The TACC domain identifies a family of centrosomal proteins that can interact with microtubules. *Proc. Natl. Acad. Sci. U.S.A.* **97**, 14352–14357 (2000). doi: [10.1073/pnas.97.26.14352](https://doi.org/10.1073/pnas.97.26.14352); pmid: [11210138](https://pubmed.ncbi.nlm.nih.gov/11210138/)
29. F. Gergely, V. M. Draviam, J. W. Raff, The ch-TOG/XMAP215 protein is essential for spindle pole organization in human somatic cells. *Genes Dev.* **17**, 336–341 (2003). doi: [10.1101/gad.245603](https://doi.org/10.1101/gad.245603); pmid: [12569123](https://pubmed.ncbi.nlm.nih.gov/12569123/)
30. C. H. Lin, C. K. Hu, H. M. Shih, Clathrin heavy chain mediates TACC3 targeting to mitotic spindles to ensure spindle stability. *J. Cell Biol.* **189**, 1097–1105 (2010). doi: [10.1083/jcb.200911120](https://doi.org/10.1083/jcb.200911120); pmid: [20566684](https://pubmed.ncbi.nlm.nih.gov/20566684/)
31. S. Petry, R. D. Vale, Microtubule nucleation at the centrosome and beyond. *Nat. Cell Biol.* **17**, 1089–1093 (2015). doi: [10.1038/ncb3220](https://doi.org/10.1038/ncb3220); pmid: [26316453](https://pubmed.ncbi.nlm.nih.gov/26316453/)
32. A. Thawani, R. S. Kadzik, S. Petry, XMAP215 is a microtubule nucleation factor that functions synergistically with the  $\gamma$ -tubulin ring complex. *Nat. Cell Biol.* **20**, 575–585 (2018). doi: [10.1038/s41556-018-0091-6](https://doi.org/10.1038/s41556-018-0091-6); pmid: [29695792](https://pubmed.ncbi.nlm.nih.gov/29695792/)
33. G. J. Brouhard *et al.*, XMAP215 is a processive microtubule polymerase. *Cell* **132**, 79–88 (2008). doi: [10.1016/j.cell.2007.11.043](https://doi.org/10.1016/j.cell.2007.11.043); pmid: [18919222](https://pubmed.ncbi.nlm.nih.gov/18919222/)
34. W. Fu *et al.*, Self-assembly and sorting of acentrosomal microtubules by TACC3 facilitate kinetochore capture during the mitotic spindle assembly. *Proc. Natl. Acad. Sci. U.S.A.* **110**, 15295–15300 (2013). doi: [10.1073/pnas.1312382110](https://doi.org/10.1073/pnas.1312382110); pmid: [24003142](https://pubmed.ncbi.nlm.nih.gov/24003142/)
35. J. Cesario, K. S. McKim, RanGTP is required for meiotic spindle organization and the initiation of embryonic development in *Drosophila*. *J. Cell Sci.* **124**, 3797–3810 (2011). doi: [10.1242/jcs.084855](https://doi.org/10.1242/jcs.084855); pmid: [22100918](https://pubmed.ncbi.nlm.nih.gov/22100918/)
36. J. Dumont *et al.*, A centriole- and RanGTP-independent spindle assembly pathway in meiosis I of vertebrate oocytes. *J. Cell Biol.* **176**, 295–305 (2007). doi: [10.1083/jcb.200605199](https://doi.org/10.1083/jcb.200605199); pmid: [17261848](https://pubmed.ncbi.nlm.nih.gov/17261848/)
37. C. So, S. Cheng, M. Schuh, Phase separation during germline development. *Trends Cell Biol.* **31**, 254–268 (2021). doi: [10.1016/j.tcb.2020.12.004](https://doi.org/10.1016/j.tcb.2020.12.004); pmid: [33455855](https://pubmed.ncbi.nlm.nih.gov/33455855/)
38. A. Webster, M. Schuh, Mechanisms of aneuploidy in human eggs. *Trends Cell Biol.* **27**, 55–68 (2017). doi: [10.1016/j.tcb.2016.09.002](https://doi.org/10.1016/j.tcb.2016.09.002); pmid: [27773484](https://pubmed.ncbi.nlm.nih.gov/27773484/)
39. S. Doubilet, K. S. McKim, Spindle assembly in the oocytes of mouse and *Drosophila*—similar solutions to a problem. *Chromosome Res.* **15**, 681–696 (2007). doi: [10.1007/s10577-007-1148-8](https://doi.org/10.1007/s10577-007-1148-8); pmid: [17674154](https://pubmed.ncbi.nlm.nih.gov/17674154/)
40. I. Peset *et al.*, Function and regulation of Maskin, a TACC family protein, in microtubule growth during mitosis. *J. Cell Biol.* **170**, 1057–1066 (2005). doi: [10.1083/jcb.200504037](https://doi.org/10.1083/jcb.200504037); pmid: [16172207](https://pubmed.ncbi.nlm.nih.gov/16172207/)
41. I. Peset, I. Vernos, The TACC proteins: TACC-ling microtubule dynamics and centrosome function. *Trends Cell Biol.* **18**, 379–388 (2008). doi: [10.1016/j.tcb.2008.06.005](https://doi.org/10.1016/j.tcb.2008.06.005); pmid: [18656360](https://pubmed.ncbi.nlm.nih.gov/18656360/)
42. D. G. Booth, F. E. Hood, I. A. Prior, S. J. Royle, A TACC3/ch-TOG/clathrin complex stabilizes kinetochore fibres by inter-microtubule bridging. *EMBO J.* **30**, 906–919 (2011). doi: [10.1038/embj.2011.15](https://doi.org/10.1038/embj.2011.15); pmid: [21297582](https://pubmed.ncbi.nlm.nih.gov/21297582/)
43. R. Yao *et al.*, A small compound targeting TACC3 revealed its different spatiotemporal contributions for spindle assembly in cancer cells. *Oncogene* **33**, 4242–4252 (2014). doi: [10.1038/onc.2013.382](https://doi.org/10.1038/onc.2013.382); pmid: [24077290](https://pubmed.ncbi.nlm.nih.gov/24077290/)
44. P. Singh, G. E. Thomas, K. K. Gireesh, T. K. Manna, TACC3 protein regulates microtubule nucleation by affecting  $\gamma$ -tubulin ring complexes. *J. Biol. Chem.* **289**, 31719–31735 (2014). doi: [10.1074/jbc.M114.57100](https://doi.org/10.1074/jbc.M114.57100); pmid: [25246530](https://pubmed.ncbi.nlm.nih.gov/25246530/)
45. T. V. Suhal, P. Singh, T. K. Manna, Suppression of centrosome protein TACC3 induces G1 arrest and cell death through activation of p38-p53-p21 stress signaling pathway. *Eur. J. Cell Biol.* **94**, 90–100 (2015). doi: [10.1016/j.ejcb.2014.12.001](https://doi.org/10.1016/j.ejcb.2014.12.001); pmid: [25613365](https://pubmed.ncbi.nlm.nih.gov/25613365/)
46. J. Roostalu, N. I. Cade, T. Surrey, Complementary activities of TPX2 and chTOG constitute an efficient importin-regulated microtubule nucleation module. *Nat. Cell Biol.* **17**, 1422–1434 (2015). doi: [10.1038/ncb3241](https://doi.org/10.1038/ncb3241); pmid: [26414402](https://pubmed.ncbi.nlm.nih.gov/26414402/)
47. P. R. Clarke, C. Zhang, Spatial and temporal coordination of mitosis by Ran GTPase. *Nat. Rev. Mol. Cell Biol.* **9**, 464–477 (2008). doi: [10.1038/nrm2410](https://doi.org/10.1038/nrm2410); pmid: [18478030](https://pubmed.ncbi.nlm.nih.gov/18478030/)
48. O. J. Gruss *et al.*, Ran induces spindle assembly by reversing the inhibitory effect of importin  $\alpha$  on TPX2 activity. *Cell* **104**, 83–93 (2001). doi: [10.1016/S0092-8674\(01\)00193-3](https://doi.org/10.1016/S0092-8674(01)00193-3); pmid: [11613242](https://pubmed.ncbi.nlm.nih.gov/11613242/)
49. P. Kalab, R. Head, The RanGTP gradient – a GPS for the mitotic spindle. *J. Cell Sci.* **121**, 1577–1586 (2008). doi: [10.1242/jcs.005959](https://doi.org/10.1242/jcs.005959); pmid: [18469014](https://pubmed.ncbi.nlm.nih.gov/18469014/)
50. R. Feng *et al.*, Mutations in *TUBB8* and human oocyte meiotic arrest. *N. Engl. J. Med.* **374**, 223–232 (2016). doi: [10.1056/NEJMoa1510791](https://doi.org/10.1056/NEJMoa1510791); pmid: [26789871](https://pubmed.ncbi.nlm.nih.gov/26789871/)

## ACKNOWLEDGMENTS

We thank all the patients and volunteers who participated in this study. We thank J. Dai from the Shanghai Academy of Agricultural Sciences for providing the porcine ovaries. We thank C. Zhang from Peking University for the gift of the human TACC3 construct. We thank K. Qiao from the Cell Biological Imaging Core Facility of IMIB at Fudan University for assistance with imaging. We are grateful to X. Li (ZEISS) for technical support with confocal live-oocyte time-lapse imaging. **Funding:** This work was supported by the National Key Research and Development Program of China (2021YFC2700100), the Basic Science Center Program of the National Natural Science Foundation of China (82288102), the National Natural Science Foundation of China (81725006, 32130029, 82101737, 82171643, 81971450, and 81971382), the Shanghai Municipal Science and Technology Major Project (2017SHZDZX01), the Project of the Shanghai Municipal Science and Technology Commission (21XD1420300), the Capacity Building Planning Program for the Shanghai Women and Children's Health Service, and the collaborative innovation center project construction for Shanghai Women and Children's Health. **Ethics statement:** The studies involving human participants were reviewed and approved by the ethics committee of the Shanghai Ji Ai Genetics and IVF Institute (JAI E2020-23 and JAI E2022-05), the ethics committee of the International Peace Maternity and Child Health Hospital (GKLW 2021-18), and the ethics committee of Fudan University (FE21198 and 2020-012). The patients and participants provided their written informed consent to participate in this study. The animal study was reviewed and approved by the animal welfare and ethics group of the Department of Experimental Animal Science of Fudan University (2017 1350 A265). **Author contributions:** T.W., J.D., J.F., and Y.K. contributed equally to this work. L.W., Q.S., and X.S. conceived of and designed the research study. T.W. designed the experiments and the methods for data analysis. T.W., J.D., Y.K., and H.G. performed the experiments. Y.L. and R.G. helped with the molecular work and genome sequencing. J.F., M.Z., and W.L. helped with human oocyte sample collection and manipulation. X.D. helped with human oocyte in vitro maturation. B.C. organized the medical records and analyzed the whole-exome data. L.W., Q.S., and T.W. drafted and revised the manuscript. **Competing interests:** The authors declare no competing interests. **Data and materials availability:** All data in the paper are present in the paper or the supplementary materials. In addition, the variation data reported in this paper

have been deposited in the Genome Variation Map of the National Genomics Data Center, China National Center for Bioinformation/Beijing Institute of Genomics, Chinese Academy of Sciences, under accession numbers GVM000402 (patients) and GVM000394 (controls). **License information:** Copyright © 2022 the authors; some rights reserved; exclusive licensee American Association for the Advancement of Science. No claim

to original US government works. <https://www.science.org/about/science-licenses-journal-article-reuse>

#### SUPPLEMENTARY MATERIALS

[science.org/doi/10.1126/science.abq7361](https://science.org/doi/10.1126/science.abq7361)  
Figs. S1 to S11  
Tables S1 and S2

MDAR Reproducibility Checklist  
Movies S1 to S5

[View/request a protocol for this paper from Bio-protocol.](#)  
Submitted 27 April 2022; resubmitted 24 August 2022  
Accepted 14 October 2022  
10.1126/science.abq7361